Pergamon

*Int. J. Solids Structures* Vol. 34, No. 4, pp. 509–525, 1997

0020–7683/97 $17.00 + .00

PII: S0020–7683(96)00026–1

# USING THE FRACTURE EFFICIENCY TO COMPARE ADHESION TESTS

YEH-HUNG LAI† and DAVID A. DILLARD‡
Engineering Science and Mechanics Department, Virginia Polytechnic Institute and State University, Blacksburg, VA 24061-0219, U.S.A.

(*Received* 29 *October* 1994; *in revised form* 29 *January* 1996)

**Abstract**—This paper reports the use of a novel concept, the fracture efficiency, to evaluate adhesion tests by deciding whether a particular test would be more or less likely to cause gross yielding or rupturing in the adherend/coating before the fracture condition is satisfied. Because of the technical importance and the difficulty in obtaining meaningful debond energies for coatings, much of the paper is devoted to the coating adhesion measurement problem. The fracture efficiency of the general coating delamination configuration is investigated and its theoretical limit is determined. The study suggests that it is unlikely to devise a new test with a significantly higher fracture efficiency than the existing tests. New experimental or analytical techniques considering the inelastic energy dissipation are needed for coating adhesion measurement. In addition to the fracture efficiency, the fracture mode mixity of the general coating delamination problem is also investigated. The conditions which may result in the contact of crack surfaces near the crack tip region are identified. The preferred configurations which would tend to induce interfacial delamination are also discussed. Finally, from the viewpoint of fracture efficiency, guidelines are given to aid in the selection of appropriate test geometries for coating adhesion measurement. Copyright © 1996 Elsevier Science Ltd.

## INTRODUCTION

A large number of fracture tests for measuring the fracture strength of adhesively bonded assemblies have been developed over the years. These tests may be conveniently grouped into three categories: laminated beam tests, blister/peel tests, and miscellaneous tests. The laminated beam tests consist of adherends which are loaded so that they behave like beams. This category includes the double cantilever beam tests of various loading modes, end notched flexure, end notched cantilever, mixed mode flexure, and four point bend tests. Blister/peel tests consist of an adherend (or a coating) bonded (or adhering) to a substrate which usually has a much higher rigidity than the peeled adherend. This category includes peel tests of various peel angles and blister tests such as Dannenberg's blister test, the standard circular blister, constrained blister, strip blister, island blister, and peninsula blister tests. When the bending stiffness of the thin adherend is negligible, and it behaves as a membrane loaded in tension, the debonding of the adherend is like the peeling of a membrane from the substrate. Therefore, this type of blister/peel test is called a "membrane peeling tests" in this paper. Other fracture tests not belonging to the previous two categories may be grouped together as miscellaneous tests, including the compact tension, compact shear, cone, Brazil nut sandwiches, indentation tests, etc. Excellent sources with references to most of these tests can be found in Brinson (1990).

One condition for successful fracture testing is to induce debonding without rupturing the adherend or the coating. When the specimen is debonded, analysis methods are then applied to determine the debond energy. Most of the analyses reported for the current fracture tests are based on the assumption that the adherends or coatings are loaded within the elastic range. These elastic analyses become invalid when general yielding occurs in the adherend. Therefore, the accuracy of using these elastic analyses depends on the extent of yielding. Only a small fraction of the literature for adhesive fracture tests has addressed the analyses of fracture specimens with general yielding. Chang *et al.* (1972) derived the energy

† Present address: Eastman Kodak Company, Rochester, New York 14650-2116, U.S.A.
‡ To whom correspondence should be addressed.

release rate for a single cantilever beam specimen with a concentrated load at the end of the adherend using an elastic-plastic model. Kim and co-workers (1988, 1989) analyzed a 90° peel test considering elastic-plastic behavior. Recently, Kinloch *et al.* (1994) extended Kim's analysis and incorporated the beam-on-elastic-foundation theory to account for the root rotation at the debonding front, resulting in a reasonable calculation of debond energy.

Although it is possible to determine the debond energy using elastic-plastic analyses when the adherend or coating yields during the debonding process, these analyses are generally more complicated and difficult to use than elastic analyses. Therefore, it is preferable to design a test that allows the specimen to be debonded without significant yielding, thus permitting the use of elastic analyses. Since fracture along the bondline and yielding/rupturing in the adherends or coatings are subject to different criteria, it is necessary to study the relationship between the quantities associated with these two different criteria in order to determine a proper specimen design that can avoid excessive yielding or rupturing. Lai and Dillard (1994) proposed a simple parameter called the fracture efficiency parameter to study the relationship between the two quantities associated with the fracture and yielding/rupturing criteria, respectively, in the standard circular and island blister tests.

In this paper, the concept of "fracture efficiency" will be further investigated by deriving this quantity for general laminated specimen consisting of two layers. These general results will then be applied to two specific classes of problems: coatings and symmetric beams. Because of their technical importance and the difficulty in obtaining meaningful debond energies for coatings in which a thin layer of material is bonded to a rather massive substrate, much of the work will be devoted to this class of problem. Through the use of nondimensionalized quantities, the most general coating configuration will be considered by examining prestresses, applied bending moments, and membrane stresses of various magnitudes and signs. This general formulation is believed to encompass most (if not all) existing and potential coating debond tests. Theoretical limits for the fracture efficiency are determined and several coating geometries are compared. Working within theoretical and practical limitations, guidelines will be given to aid in the selection of appropriate test geometries. The paper will close with a comparison of several loading methods for symmetric beam specimens, where again the fracture efficiency will be shown to be useful in determining the likelihood of adherend yield or rupture.

## DEFINITION OF FRACTURE EFFICIENCY PARAMETER

To determine how likely an adhesion test is to result in yielding/rupturing of the adherend or coating before the fracture (debonding) condition is met, two quantities associated with the debonding and yielding/rupturing criteria are needed. The selection of the yielding/rupturing criterion depends on the ductility of the material. An appropriate quantity may be the maximum principal stress, maximum shear stress, or maximum effective stress based on the Von Mises criterion, although other criteria could also be used. Within the framework of linear elastic fracture mechanics, a commonly used quantity associated with the fracture criterion for adhesive assemblies is the energy release rate. The energy release rate can usually account for the localized energy dissipation in the crack-tip plastic zone which can be viewed as part of the fracture energy. However, it should not be used to account for the plastic energy dissipation due to the non-singular stress such as the bending stress in a beam or plate type specimen. Therefore, when the non-singular stress exceeds the yielding stress, an energy release rate based on the elastic analysis is no longer valid. In this paper, assuming that linear elastic fracture mechanics is applicable and the crack tip plastic zone size is small, the term 'yielding' will specifically refer to the general adherend (or coating) yielding resulting from the non-singular stresses. The term 'maximum stress' will refer to the maximum non-singular stress, which is often obtained by a mechanics of materials approach. The following section will describe how these two quantities—the energy release rate and the maximum stress, can be combined to form the fracture efficiency.

In a dimensional analysis similar to the one by Broek (1982), the energy release rate, being proportional to a strain energy term and a length term, is given by

$$G = C^* \frac{\sigma_{avg}^2 \lambda^*}{E^*}, \tag{1}$$

where

$\sigma_{avg}$ is the average far field applied stress,
$E^*$ is a characteristic material modulus,
$\lambda^*$ is a characteristic length,
and $C^*$ is a nondimensional constant.

Following a similar dimensional analysis, one can express the energy release rate in terms of the maximum stress, $\sigma_{max}$, as

$$G = C_e \frac{\sigma_{max}^2 \lambda^*}{E^*}, \tag{2}$$

where $C_e$ is a nondimensional coefficient which is a function of test geometry, material properties, specimen dimensions, etc.

In eqn (2), the quantity

$$\frac{C_e \lambda^*}{E^*},$$

which is the ratio between energy release rate and the square of the maximum stress, can be used to evaluate the 'fracture efficiency' of a certain test geometry, or the ability of a test to produce a maximum energy release rate at a certain maximum stress level. This quantity is defined to be the 'fracture efficiency parameter', $T_e$, and is expressed by:

$$T_e = \frac{G}{\sigma_{max}^2}. \tag{3}$$

For simplicity, the maximum principal stress is used in the current study to include both possible yielding and rupturing cases, although stress quantities associated with other material failure criteria may be used as well.

With the fracture efficiency parameter defined, it is natural to define a critical fracture efficiency parameter as the ratio between the debond energy and the square of the critical stress for the adherend,

$$T_e^c = \frac{\Gamma}{\sigma_{cr}^2}, \tag{4}$$

where $\Gamma = \Gamma(\psi)$ is the debond energy,

$$\psi \text{ is the phase angle and is given by } \psi = \tan^{-1}\left(\frac{K_{II}}{K_I}\right), \tag{5}$$

$K_I$ and $K_{II}$ are mode I and mode II stress intensity factors, respectively, and $\sigma_{cr}$ is the critical stress (yielding or rupturing stress) in the adherend.

The fracture efficiency parameter can be normalized with respect to the critical fracture efficiency parameter. This 'normalized fracture efficiency parameter' is expressed by

$$\bar{T}_e = \frac{T_e}{T_e^c} = C_e \frac{\lambda^*}{E^*} \frac{\sigma_{cr}^2}{\Gamma}. \tag{6}$$

The normalized fracture efficiency parameter is useful both in designing the specimen and evaluating the validity of the measured debond energy. If the normalized fracture efficiency parameter is larger than unity, then the specimen should debond without adherend yielding/rupturing. To design such a specimen, one may estimate a debond energy, then choose an appropriate test geometry and design an appropriate specimen dimension to obtain a normalized fracture efficiency parameter larger than unity so that general yielding or rupturing can be prevented and the elastic solution can be used. Alternately, if the measured debond energy calculated from an elastic solution results in a normalized fracture efficiency parameter is smaller than unity, the adherend is expected to yield during debonding. In this case, one may need to use an elastic-plastic analysis to determine the debond energy, or redesign the specimen to eliminate general yielding.

To summarize, the test efficiency is a ratio of the available energy release rate to the square of the maximum (non-singular) stress associated with the given loading. This quantity is a calculated quantity which depends on the specimen geometry and loading, and the constitutive properties of the materials. The critical fracture efficiency parameter represents a ratio of the experimentally determined critical energy release rate (which may depend on the mode mixity) and the experimentally determined yield/rupture strength. The normalized fracture efficiency is a ratio of the former to the latter; a value exceeding unity suggests that debonding will occur, whereas a value less than unity implies the likelihood of yield or rupture rather than debonding.

## APPLICATION OF THE FRACTURE EFFICIENCY PARAMETER

*The fracture efficiency of general coating delamination specimens*

In this section, a general coating delamination specimen as shown in Fig. 1 is considered. A coating is adhering to a substrate with a bending rigidity much larger than the coating. At the debond front, the coating is subjected to a combined loading of in-plane force $P$ and bending moment $M$, each per unit width. The energy release rate can be obtained based on the results of Hutchinson and Suo (1992):

$$G = [(P-\sigma_0 h)^2 + 12M^2/h^2]/(2\hat{E}h), \tag{7}$$

where $\sigma_0$ is the prestress in the coating, $E$, $\nu$, and $h$ are the Young's modulus, Poisson's ratio and thickness, respectively, of the coating; for the plane strain case, $\hat{E} = E/(1-\nu^2)$ and for the plane stress case, $\hat{E} = E$.

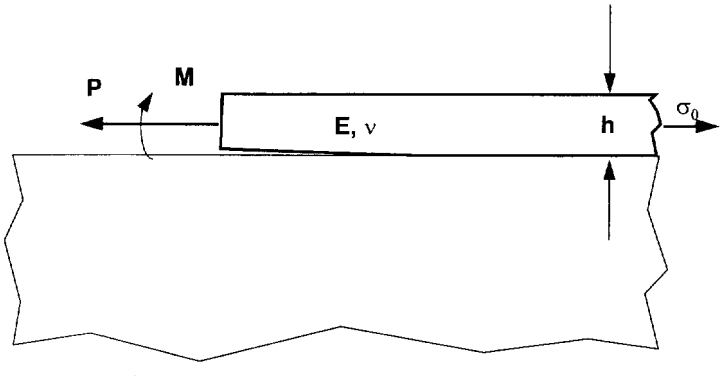


Fig. 1. A general coating delamination configuration.

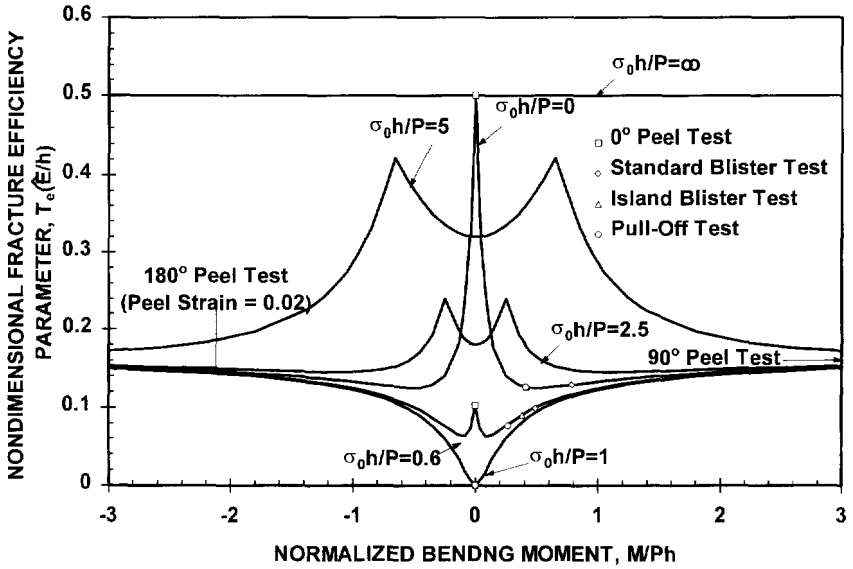


Fig. 2. Fracture efficiency in the general coating delamination specimen for several positive non-dimensional prestresses.

Since $P$ and $M$ may be applied independently, one may change the loading conditions to correspond with various membrane peeling tests, plate-like blister tests, or laminated beam tests by simply changing the ratio between $P$ and $M$. The maximum non-singular stress can be easily obtained with known values of $P$ and $M$. Alternately, if $P$, $\sigma_0$ and $G$ are known, as is often found in membrane peel and blister tests, the bending moment can be easily obtained using eqn (7).

For the general coating delamination specimen, the fracture efficiency parameter is given by

$$T_e = \min\left\{ \frac{h}{\hat{E}} \frac{\left(1-\frac{\sigma_0 h}{P}\right)^2 + 12\left(\frac{M}{Ph}\right)^2}{2\left(\left|\frac{6M}{Ph}\right|+1\right)^2}, \frac{h}{\hat{E}} \frac{\left(1-\frac{\sigma_0 h}{P}\right)^2 + 12\left(\frac{M}{Ph}\right)^2}{2\left(\frac{\sigma_0 h}{P}\right)^2} \right\}. \tag{8a}$$

or by

$$T_e = \min\left\{ \frac{h}{\hat{E}} \frac{1+12\left(\frac{M}{\sigma_0 h^2}\right)^2}{2\left(\frac{6M}{\sigma_0 h^2}\right)^2}, \frac{h}{\hat{E}} \frac{1+12\left(\frac{M}{\sigma_0 h^2}\right)^2}{2} \right\}, \quad \text{when } P = 0. \tag{8b}$$

From eqn (8a), the fracture efficiency parameter is a function of three parameters, the nondimensional moment $M/Ph$, the nondimensional prestress $\sigma_0 h/P$, and the thickness to modulus ratio $h/\hat{E}$. Figures 3–5 illustrate the nondimensional fracture efficiency parameter, $T_e\hat{E}/h$, vs nondimensional moment for the general coating delamination problem. The results in these figures cover all possible results for coating delamination test geometries with the crack tip loading condition shown in Fig. 1.

The discussion of Fig. 2 in the following paragraphs will be divided between two possible ranges of the nondimensional prestress: from 0 to 1 and 1 to $\infty$. Curves with typical nondimensional prestress will be plotted. All curves are symmetric with respect to the zero moment axis. In addition, the fracture efficiency of several membrane peeling tests will also be discussed.

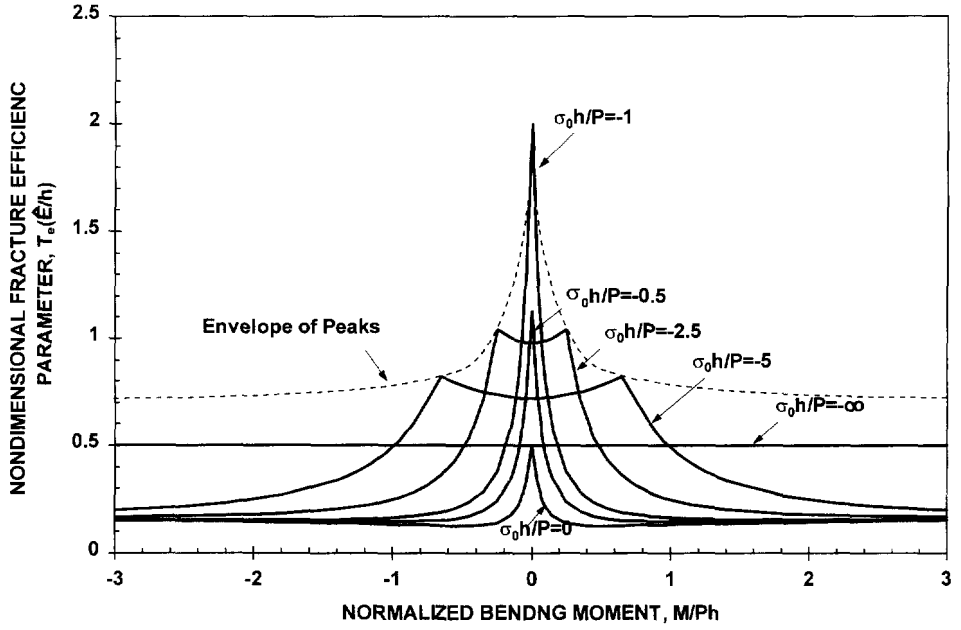


Fig. 3. Fracture efficiency in the general coating delamination specimen for several negative nondimensional prestresses.

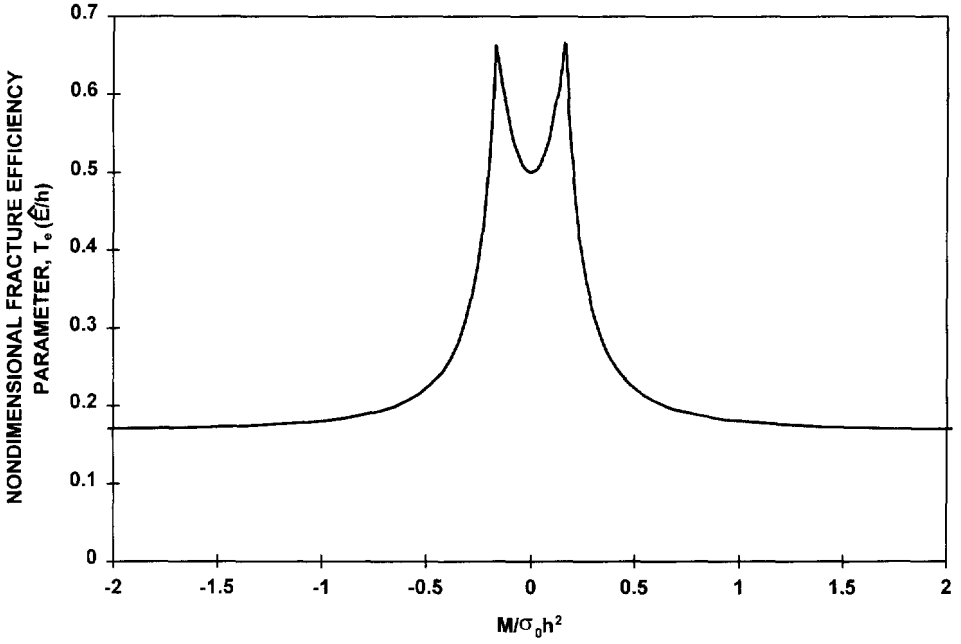


Fig. 4. Fracture efficiency in the general coating delamination specimen with zero in-plane force.

For specimens with a nondimensional prestress from 0 to 1, $T_e\hat{E}/h$ is between 0.5 and 0. One peak is seen in each $T_e\hat{E}/h$ plot, corresponding to the shift of location of the maximum stress from the upper surface to the lower surface in the debonded side of the coating. This category includes all existing membrane peeling tests with a coating prestress in tension which is probably the most commonly encountered testing configuration. Typically, it includes blister tests and peel tests with various peel angles. In this category, the curves with nondimensional prestresses of 0 and 1 are two limiting cases. Other curves with a nondimensional prestress between 0 and 1 are located between these two limiting curves. It is interesting to note that both the maximum and minimum fracture efficiency parameters occur at zero moment depending on the nondimensional prestress. For all curves, $T_e\hat{E}/h$ converges to 0.167 when the nondimensional moment is very large.

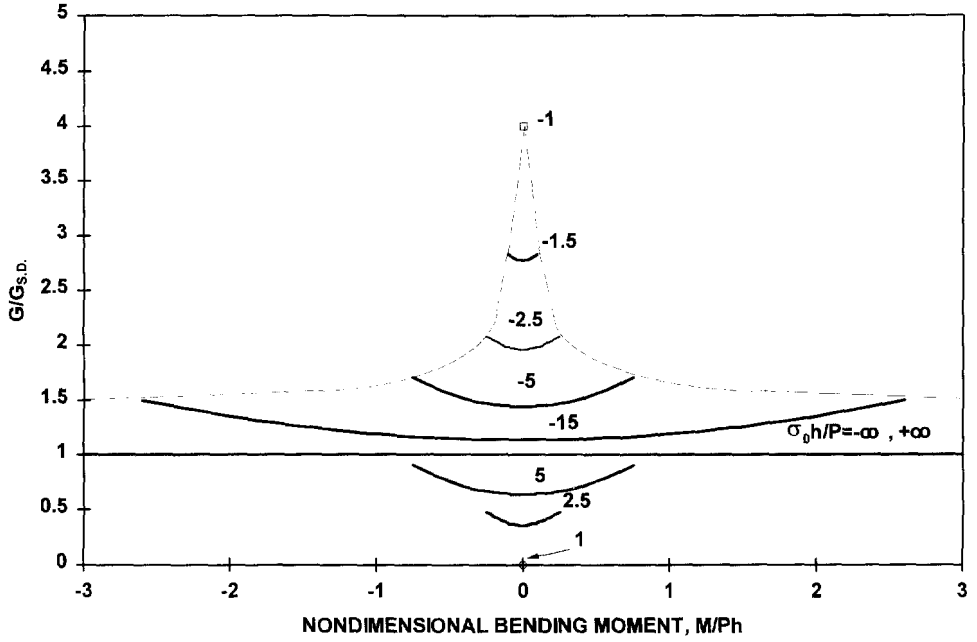


Fig. 5. The energy release rates normalized with respect to the energy release rate for the self delamination configuration.

In Fig. 2, the values of $T_c\hat{E}/h$ for several typical membrane peeling tests for coatings with a tensile or zero prestress are also marked. These tests include peel tests of 0°, 90°, and 180° peel angles, the standard blister, island blister (Allen and Senturia, 1988, 1989), and pull-off (Gent and Kaang, 1986) tests. The energy release rate and the membrane stress at the debond front of these tests can be obtained based on Lai and Dillard (1994), Anderson *et al.* (1977), and Gent and Kaang (1986). After the energy release rate and membrane stress are obtained, the bending moment can be easily determined using eqn (7). In these tests, the 0° peel test with a coating having a zero prestress has a value of 0.5 $T_c\hat{E}/h$. When the applied peel stress is equal to the prestress in a 0° peel test, the energy release rate is equal to zero and therefore, the fracture efficiency parameter is zero. It is interesting to note that the pull-off, island blister, and standard blister tests all have similar fracture efficiencies even though they have very different test geometries and loading conditions. As the nondimensional prestress increases, the fracture efficiency of these three tests decreases and then approaches zero as the nondimensional prestress approaches 1. The results suggest that when the prestress is very small, peel tests involving very small peel angles may be preferable. However, when the prestress is relatively large, high angle peel tests may be advantageous. The results for the membrane peeling tests also suggest that despite several advantages over peel tests, the blister test is more likely to initiate general yielding or rupturing compared to peel tests of high peel angles.

In Fig. 2, two peaks or cusps are observed for the cases with a nondimensional prestress from 1 to $\infty$, corresponding to shifts of the maximum stress locations from the debonded side to the bonded side (with the prestress being the maximum stress) and then back to the debonded side of the coating. $T_c\hat{E}/h$ in this nondimensional prestress range also varies between 0 and 0.5. This prestress range represents cases where the membrane stress in the debonded side has the same sign but a smaller magnitude compared with the prestress. A typical example of this case is the buckle-driven delamination of thin films (Hutchinson and Suo, 1992). For the case with a very large nondimensional prestress, $T_c\hat{E}/h$ is nearly constant with a value of 0.5, corresponding to the prestress induced self delamination test (Farris and Bauer, 1988) or notched coating adhesion test (Chang *et al.*, 1996).

Figure 3 illustrates the fracture efficiency of the coating delamination problem with a negative nondimensional prestress. This nondimensional prestress range represents the case where $P$ has a sign opposite to that of the prestress. This category includes membrane peeling tests for the coating with a compressive prestress or indentation tests (Ritter and

Rosenfeld, 1990) for the coating with a tensile prestress. One peak is seen for the curve with a nondimensional prestress from 0 to $-1$. The peak value increases from 0.5 to 2 as the nondimensional prestress decreases from 0 to $-1$. Two peaks are seen for curves with a nondimensional prestress more negative than $-1$. The peak values decrease from 2 to 0.5 as the nondimensional prestress decreases from $-1$ to $-\infty$. The envelope of the peak points is also plotted. All curves are symmetrical with respect to the axis of zero moment. At a very large nondimensional moment, $T_e\hat{E}/h$ also converges to a constant of 0.167. From Figs 3 and 4, it is seen that $T_e\hat{E}/h$ of 2 is the theoretical limit. However, this case may merely be a coincidence since if one does not obtain debonding at this combination of prestress and external load, one has to increase the load, thus causing the fracture efficiency to decrease. Therefore, this theoretical limit can not be induced in general with any test geometry.

When $P$ is zero, which is typically found in the 90° peel test, the self delamination test, and the notched coating adhesion test, eqn (8b) should be used to determine the fracture efficiency. In this case, there is only one independent loading parameter, $M/\sigma_0 h^2$. Figure 4 illustrates the fracture efficiency of this particular case. Two peaks are also seen in this curve. Higher fracture efficiencies are seen when $M/\sigma_0 h^2$ is small. When $M/\sigma_0 h^2$ is larger than 1, $T_e\hat{E}/h$ begins to approach a constant, 0.167.

From Figs 2–4, the maximum stress is the prestress for certain loading conditions, which are found in the curves with double peaks. In these cases, the coating may crack or yield in the bonded region depending on the ductility of the coating. In a brittle coating where the cracked coating may prevent the adhesion measurement, the prestress may be used as the maximum stress to determine the fracture efficiency. In a ductile coating, although the prestress in the coating may initially exceed the yield stress, no general yielding would occur during the debonding process in which the unloading of the prestress is always elastic. Therefore, the elastic solution for the energy release rate and the phase angle would be still applicable. In this case, it is more appropriate to use eqn (9) to determine the fracture efficiency parameter:

$$T_e = \frac{h}{\hat{E}} \frac{(P-\sigma_0 h)^2 + 12(M/h)^2}{2\left(\left|\frac{6M}{h}\right| + P\right)^2}, \tag{9}$$

despite the prestress is the maximum stress. It should be noted that the fracture efficiency parameter determined in this way can be as high as infinity in the case of self delamination of coatings. It may appear that a test configuration in this category would be ideal for coating adhesion testing. However, after careful examination, it is found that the usefulness of the test configuration in this category would be constrained by the range of the energy release rate rather than the fracture efficiency. When the coating does not self-delaminate, external loads are needed to supply extra energy for delamination. By comparing the energy release rate from the self delamination case and that from the case with external loads, one can determine the limitation of this test category. Figure 5 illustrates the energy release rate normalized with respect to the energy release rate in the self delamination case. The latter is given by

$$G_{S.D.} = \frac{\sigma_0^2 h}{2\hat{E}}. \tag{10}$$

Note that only the curves with the prestress being the maximum stress are shown in Fig. 5. For the case with a nondimensional prestress larger than 1, the energy release rate is smaller than $G_{S.D.}$, which suggests that if the coating does not self delaminate, one can not initiate fracture while keeping the maximum stress in the debonded region. For the case with a nondimensional prestress smaller than $-1$, a higher energy release rate than $G_{S.D.}$ can be obtained. However, the limit is $4G_{S.D.}$, which corresponds to the case with a nondimensional

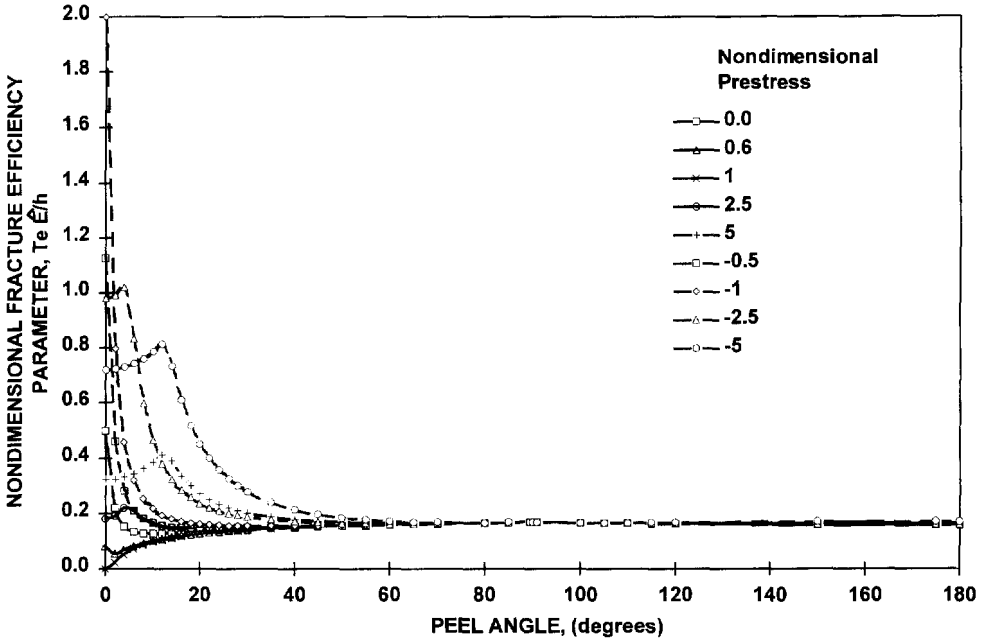


Fig. 6. Fracture efficiency in the peel test with various peel angles and prestresses.

prestress of $-1$ and a moment of 0. Note that this case is exactly the same as the one with the theoretical limit of the fracture efficiency as shown in Fig. 3. When debonding is not obtained at this combination of prestress and external load, one has to increase the energy release rate by increasing the external load, which would then move the maximum stress to the debonded region and result in a lower fracture efficiency.

Because of the theoretical limit of fracture efficiency in the most general coating delamination configuration, general yielding or rupturing can not be prevented for a given coating thickness. Furthermore, it may be useless to devise a new test configuration or switch among existing test configurations. One may need to increase the coating thickness significantly to increase the fracture efficiency or to analyze the results by accounting for the yielding. Another possible way to avoid general yielding is to conduct the test by applying a backing at the top of the coating. From the viewpoint of fracture efficiency, a successful backing material should have a small modulus, a high yielding stress, or a sufficient large thickness. This can be easily seen from the expression of the normalized fracture efficiency parameter, eqn (6).

Figure 6 illustrates the fracture efficiency versus peel angle of the peel test with various nondimensional prestresses for a typical peel strain of 0.01. The energy release rate for the general peel tests is taken from eqn (20) of the paper by Thouless and Jensen (1992). With the known energy release rate, applied peel strain and peel angle, the fracture efficiency parameter can be easily obtained. Nondimensional prestress found in Figs 3 and 4 are used. It is seen that when the peel angle approaches 90°, $T_e\hat{E}/h$ converges at 0.167. For small peel angles, $T_e\hat{E}/h$ has large variations for different nondimensional prestresses. As expected, the case with a negative nondimensional prestress and small peel angles have a relatively large $T_e\hat{E}/h$.

*The mode mixity of general coating delamination specimens*

In recent years, it has been established that one can not fully understand the measured debond energy without an understanding of the fracture mode mixity induced in the test (Hutchinson and Suo, 1992). In this section, the fracture mode will be investigated through a study of phase angles (eqn (5)). Based on Hutchinson and Suo, the phase angle for a general coating delamination specimen can be easily derived and is given by

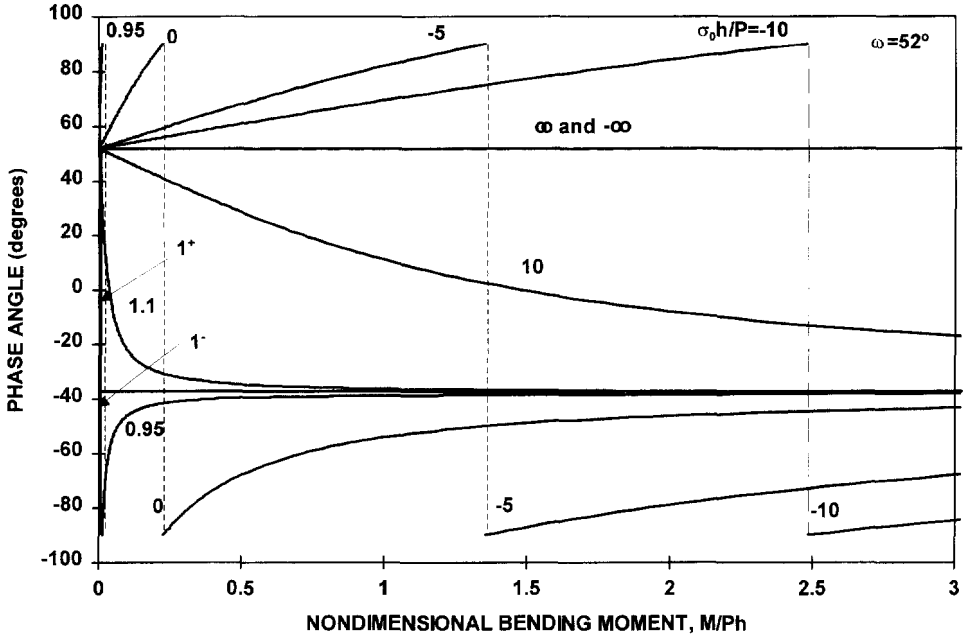


Fig. 7. Phase angles of the general coating delamination specimen for positive nondimensional moments and various nondimensional prestresses.

$$\psi = \frac{\sqrt{12}\dfrac{M}{Ph}\dfrac{1}{1-\sigma_0 h/P}+\tan\omega}{-\sqrt{12}\dfrac{M}{Ph}\dfrac{1}{1-\sigma_0 h/P}\tan\omega+1}, \tag{11}$$

or by

$$\psi = \frac{-\sqrt{12}\dfrac{M}{\sigma_0 h^2}+\tan\omega}{\sqrt{12}\dfrac{M}{\sigma_0 h^2}\tan\omega+1}, \quad \text{when } P=0, \tag{12}$$

where $\omega$ is a function of bi-material properties which has been tabulated by Hutchinson and Suo. Following the sign convention of Hutchinson and Suo, it is found that the crack surfaces near the tip would open if $K_{\mathrm{I}}$ is positive. When $K_{\mathrm{I}}$ is negative, the crack surfaces close and contact. The analysis of fracture under this condition may need to include the effect of friction between the crack surfaces within the crack tip contact zone (Thouless *et al.*, 1992). The sign convention also dictates that the crack would tend to grow upward when $K_{\mathrm{II}}$ is negative.

Figure 7 illustrates the phase angle for the coating delamination specimens with a positive nondimensional moment. A typical $\omega$ of 52° is used. Two distinct patterns for the phase angle are found depending on whether the nondimensional prestress is smaller or larger than 1. When the nondimensional prestress is larger than 1, the phase angle distribution is continuous throughout the positive range of nondimensional moment. For a nondimensional prestress smaller than 1, there is a discontinuity and a sudden reversal of sign in the phase angle. These discontinuities occur when phase angles change from positive 90° to negative 90°, which corresponds to the change of $K_{\mathrm{I}}$ from $0^+$ to $0^-$ or vice versa. The change in the sign of $K_{\mathrm{I}}$ also represents the situation in which the crack surface near the crack tip changes from opening mode to closing mode. When the nondimensional prestress is larger than 1, the sign of phase angle may also change. However, this change of sign is associated with the sign change in $K_{\mathrm{II}}$. It should be noted that a sign change of $K_{\mathrm{II}}$ would

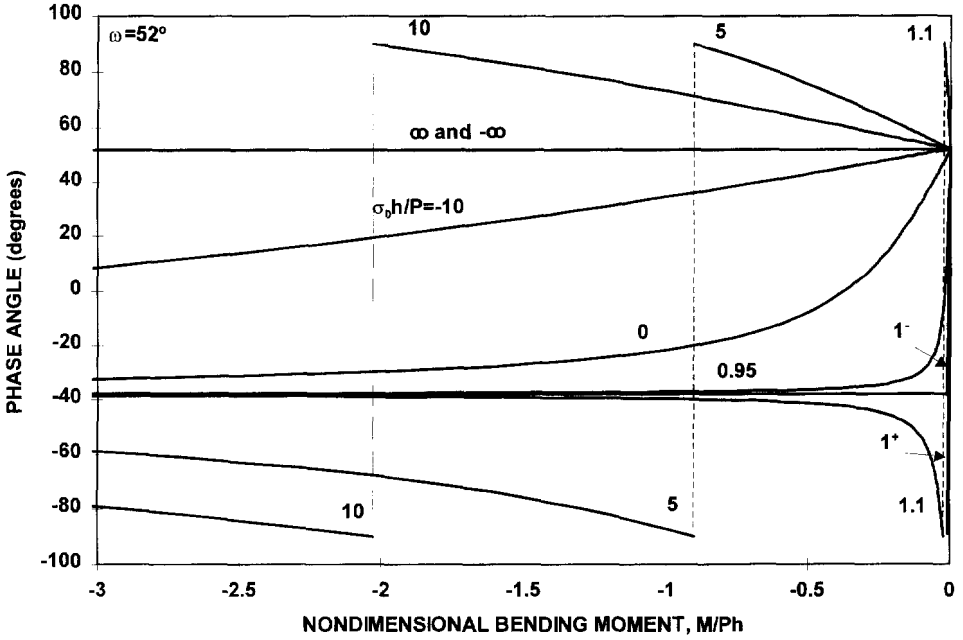


Fig. 8. Phase angles of the general coating delamination specimen for negative nondimensional moments and various nondimensional prestresses.

change the tendency of crack growth direction. It is interesting to note that pure mode I fracture can be achieved in this nondimensional prestress range. In this nondimensional prestress range, crack surfaces would remain open or closed for all nondimensional moments. For all nondimensional prestresses, the phase angle would converge to $\omega$ at zero bending moment and to $-38^\circ$ at a very large bending moment. The result of the zero prestress is consistent with the study of peel geometries by Thouless and Jensen (1992) who found that the phase angle is essentially constant except at a very small peel angle.

Figure 8 has similar results as those in Fig. 7 but for negative values of the nondimensional moment. However, unlike in Fig. 7, discontinuity of the phase angle distribution is seen for the curve with a nondimensional prestress larger than 1. The phase angle also converges to $\omega$ at zero moment and to $38^\circ$ at a very large bending moment.

When $P$ is zero, eqn (12) should be used to determine the phase angle, the results of which are shown in Fig. 9. The independent loading parameter is $M/\sigma_0 h^2$. A discontinuity is found when $M/\sigma_0 h^2$ is equal to $-0.226$. When $M/\sigma_0 h^2$ is smaller than $-0.226$, the phase angle is negative. When $M/\sigma_0 h^2$ is larger than $-0.226$, the phase angle decreases from $90^\circ$, and eventually plateaus out at $-38^\circ$ for large nondimensional moments. It should be noted that unlike the fracture efficiency plot, the phase angle plot is not symmetric with respect to the zero bending moment. The result of the phase angle study shown in Figs 7–9 provides a convenient method to choose a test configuration that would tend to debond the specimen at the desired location. For example, a test with a positive $K_{II}$ would have a better chance of inducing interfacial debonding than one with a negative $K_{II}$.

*The effect of mode mixity on the fracture efficiency of the symmetric beams*

Although it is possible to study the fracture efficiency considering the fracture mode, in this paper, we will only attempt to demonstrate how the fracture mode can be considered in determining the fracture efficiency by comparing four laminated beam specimens with different fracture modes. These four specimens are the double cantilever beam (DCB), end loaded split (ELS), four point bend (FPB), and cracked lap shear (CLS) specimens as shown in Fig. 10. The first three specimens are subjected to pure bending loads at the ends of the adherends. A symmetrically loaded double cantilever beam specimen has $M_1 = M_2$. An end loaded split specimen has $M_1 = -M_2$. A four point bend specimen has $M_2 = 0$. The cracked lap shear specimen is subject to an axial load at each end. The cracked lap shear specimen is assumed to be very long compared to the total specimen thickness and is

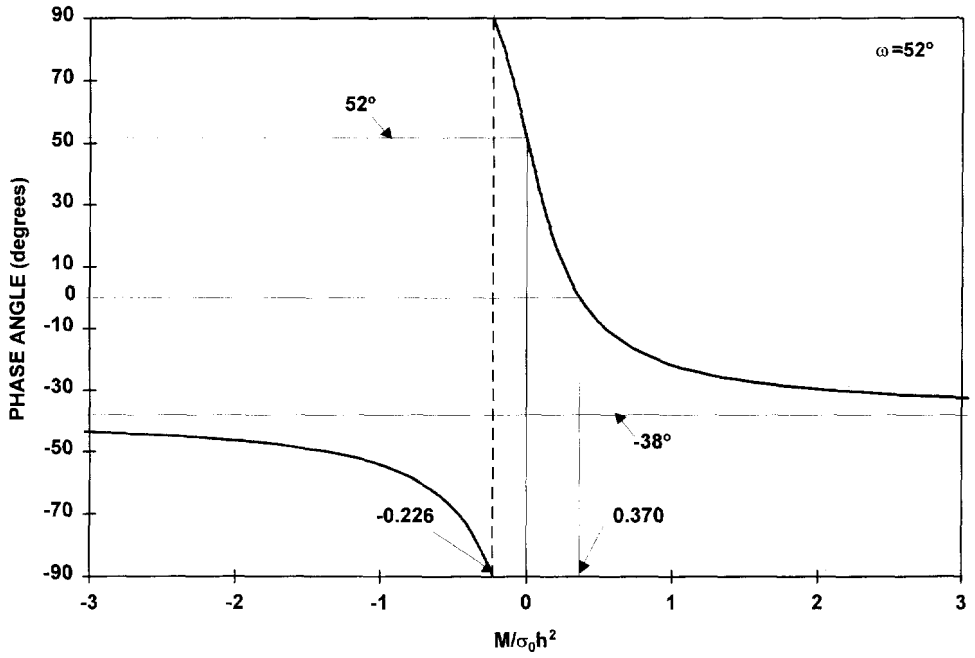


Fig. 9. Phase angles of the general coating delamination specimen with a zero resultant in-plane stress.

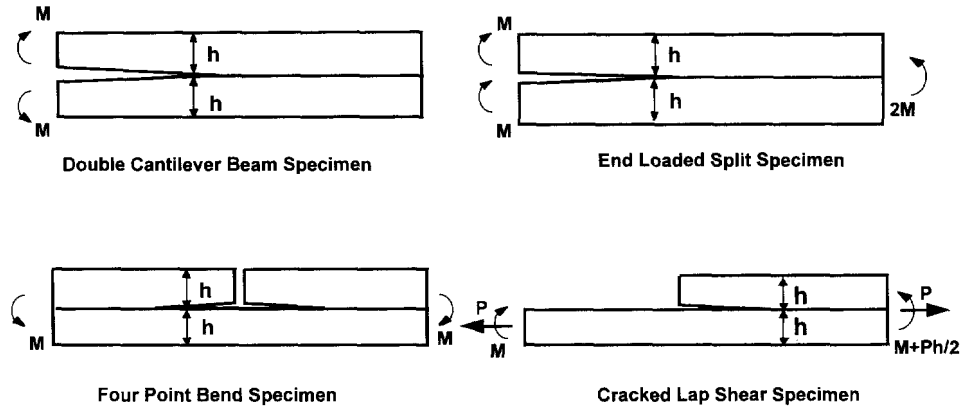


Fig. 10. Four typical laminated beam specimens.

subjected to an axial load, which results in a constant energy release rate and constant fracture efficiency parameter test (Lai and Dillard, 1996). It should be noted that bending moments are added in the illustration of CLS specimen in order to represent the realistic loading condition near the debond front. All specimens are assumed to be made of the same material and equal thickness for the top and bottom adherends. A mixed mode fracture criterion proposed by Hutchinson and Suo (1992) may be used:

$$\Gamma(\psi) = G_i^c[1+\tan^2(1-\lambda)\psi], \tag{13}$$

where $\Gamma(\psi)$ is the debond energy function, $G_i^c$ is the debond energy at pure mode I, and $\lambda$ is a parameter that adjusts the influence of mode mixity and should be determined by experiment.

Table 1 tabulates the fracture efficiency parameter and phase angle for the four laminated beam specimens shown in Fig. 10. The phase angles for the DCB, ELS, and FPB specimens can be easily determined from Hutchinson and Suo (1992). The phase angle for the CLS specimen is obtained from Lai and Dillard (1996).

Table 1. Fracture efficiency parameters and phase angles for four laminated beam specimens

| | DCB | ELS | FPB | CLS |
|---|---|---|---|---|
| $T_e$ | $\frac{1}{3}\frac{h}{E}$ | $\frac{1}{4}\frac{h}{E}$ | $\frac{7}{48}\frac{h}{E}$ | $\frac{9+4\sqrt{2}}{32(3+2\sqrt{2})}\frac{h}{E}$ |
| $\psi$ | 0° | 90° | 40° | 63° |

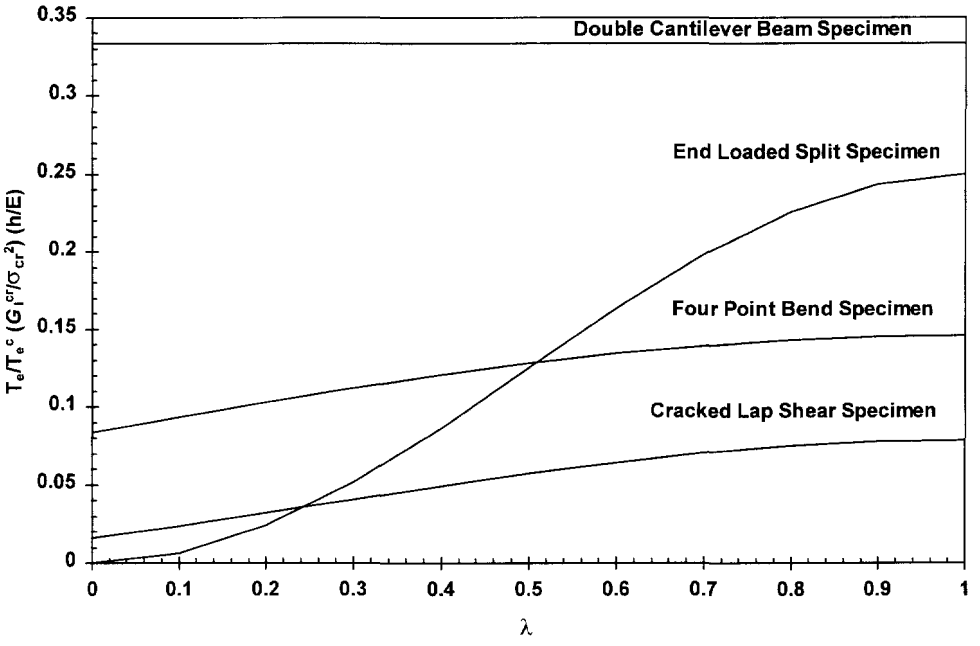


Fig. 11. Ratio between the fracture efficiency parameter and critical fracture efficiency parameter for laminated beam specimens as a function of $\lambda$.

Figure 11 illustrates the effect of the phase angle on the fracture efficiency. The ordinate is represented by $T_e(G_I^c h/\sigma_{cr}^2 E)$. Since $\lambda$ adjusts the contribution of the mode II debond energy, the fracture efficiency of the mode I DCB test is independent of $\lambda$, while the fracture efficiency of the mode II ELS specimen is very small for a small $\lambda$. As $\lambda$ increases, the fracture efficiency of the ELS, FPB, and CLS specimens increases. To successfully debond a specimen without causing yielding, one needs to design a specimen that has a normalized fracture efficiency parameter larger than 1. For the current specimens, the normalized fracture efficiency parameter depends on the values of $(h/E)(\sigma_{cr}^2/G_I^c)$ and $\lambda$. For example, to measure the debond energy for a typical material system with a $\lambda$ equal to 0.3, $(h/E)(\sigma_{cr}^2/G_I^c)$ should be greater than 3 for a double cantilever beam specimen, 8.9 for the FPB specimen, 19.4 for the ELS specimen, and 24.7 for the CLS specimen. The comparison suggests that from the viewpoint of fracture efficiency, the double cantilever beam specimen is the best one of the four. It should be noted that comparisons are useful as one determines appropriate specimen dimensions, although the desire for a particular mode mix may ultimately dictate the choice of specimens. The fracture efficiency of coating delamination specimens can be compared in a similar manner to that demonstrated in this example, however, the independent parameters would be three instead of one.

*Selection and design guidelines for coating adhesion tests*

Based on the current study, guidelines are established to aid in the selection and design of appropriate test geometries for coatings from the viewpoint of the fracture efficiency:

1. The self delamination test is a good starting point in measuring coating adhesion if self delamination can be successfully induced and the coating prestress can be properly determined. To induce self delamination, a relatively high prestress or thick coating is needed for systems with strong adhesion. When the coating does not self delaminate, an external loading can be used in tests such as the notched coating adhesion test to increase the coating stress in the bonded section and therefore achieve the effect of self delamination.
2. When the coating prestress is in tension, tests which can induce compressive stresses in the debonded portion of coatings are preferred because a relatively large non-dimensional fracture efficiency (larger than 0.5) can be achieved. A typical test in this class is the indentation test.
3. Similarly, when the coating prestress is in compression, tests inducing tensile stresses in the debonded portion of the coating are preferred. Typical tests are peel tests of low angle and blister tests.
4. In membrane peeling tests, the peel test with a very low peel angle performs better when the prestress is in compression or very small in tension. Alternatively, the peel test with a large peel angle (larger than 60°) should be a better choice for the sample with a relatively large tensile prestress. For samples with tensile prestresses, blister tests give a smaller fracture efficiency than peel tests with large peel angle. Therefore, from the viewpoint of fracture efficiency, large peel angle tests are more desirable than blister tests in this case.
5. When it is possible, one could increase the coating thickness or use a proper backing.
6. In addition to the tendency of crack growing direction, one should also consider the effect of the fracture mode mixity on the fracture efficiency.
7. If the yielding problem can not be prevented, one should use an elastic-plastic analysis to interpret the test results.

*Error study of using elastic solutions when yielding occurs*

In the previous discussions, the focus was on designing a specimen with a high fracture efficiency so that the elastic solutions could be applied to determine the debond energy. When the normalized fracture efficiency parameter is smaller than unity, yielding may occur and the debond energy based on the elastic solution would be in error. An error study of debond energy measurement in two typical fracture tests, the double cantilever beam test and the 90° peel test, is illustrated in Figs 12 and 13 for the case in which the normalized fracture efficiency parameters are smaller than unity. The notation, $G_{el}$, denotes the energy release rate obtained from an elastic analysis even though the specimen may have yielded. The notation, $G_y$, denotes the energy release rate obtained from a solution which correctly accounts for the plastic deformation. Deviation of the $G_{el}$ to $G_y$ ratio from unity indicates the magnitude of the potential error resulting from an elastic analysis.

In Fig. 12, $G_y$ is obtained from a double cantilever beam solution with concentrated loads applied at the ends of the adherends. It is noted that $G_{ym}$ is simply twice that derived by Chang *et al.* (1972) for a single cantilever beam specimen. The adherends are assumed to be isotropic, homogeneous, and elastic-perfectly plastic. The error is zero when the normalized fracture efficiency parameter is larger than 1, which indicates that the maximum bending stress is smaller than the yield stress during debonding. When the normalized fracture efficiency parameter is smaller than 1, the adherend yields. It is interesting to see that $G_{ym}$ is larger than $G_{el}$ when yielding occurs, which suggests that although some energy is dissipated in the plastic deformation, more work is done in the system because yielding results in a larger displacement at the end of the adherend where the load is applied. The ratio between $G_{el}$ and $G_{ym}$ decreases as the normalized fracture efficiency parameter decreases. When the normalized fracture efficiency parameter is smaller than 0.444, plastic hinges form and the analysis for $G_{ym}$ by Change *et al.* is no longer valid. When the normalized fracture efficiency parameter is larger than 0.5, the error is smaller than 20%. When the normalized fracture efficiency parameter is smaller than 0.5, the error increases rapidly.

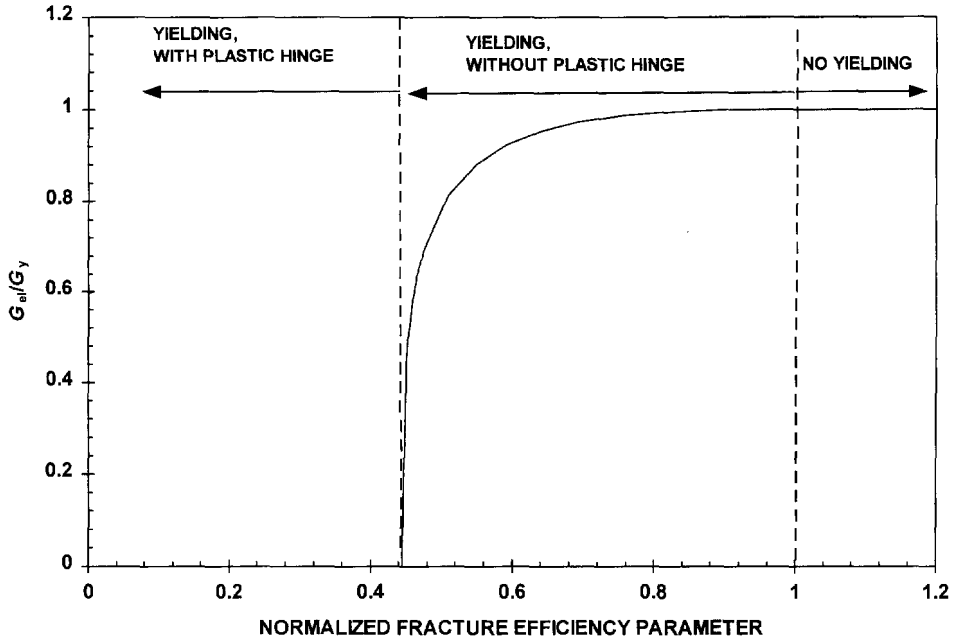


Fig. 12. An error study of using the elastic solution for a double cantilever beam specimen when the adherend yields.

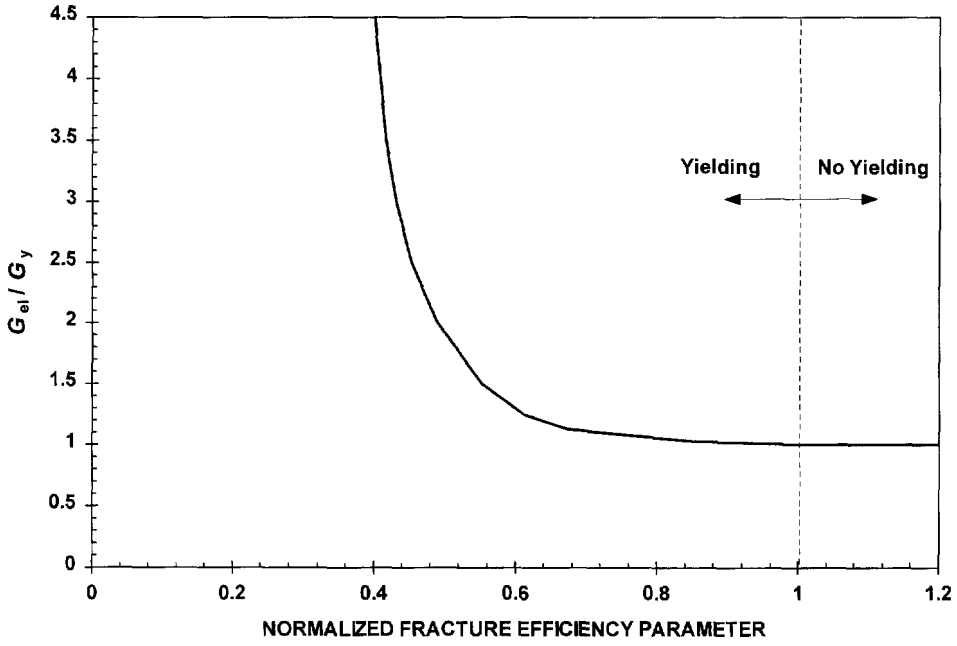


Fig. 13. An error study of using the elastic solution for a 90° peel test when the coating yields.

Figure 12 illustrates an error study of the 90° peel test for various normalized fracture efficiency parameters. The $G_{ym}$ is obtained from the solution by Kim *et al.* (1988, 1989) for an elastic-perfectly plastic peel specimen. It is interesting to note that the normalized fracture efficiency parameter in the 90° peel test is equivalent to the "normalized thickness" in Kim's paper and therefore, the result of $G_{el}$ to $G_{ym}$ ratio is the same. The specimen yields when the normalized fracture efficiency parameter is smaller than 1. It is also interesting to note that, contrary to the double cantilever beam specimen discussed in Fig. 12, the ratio between $G_{el}$ and $G_{ym}$ increases as the normalized fracture efficiency parameter decreases, which suggests that increasingly more energy is dissipated due to the plastic deformation than debonding as the normalized fracture efficiency parameter decreases. The different

trend in the 90° peel test may be explained in that the inelastic energy is dissipated in bending, which does not permit additional axial deformation, so there is no additional energy input as in the double cantilever beam specimen. When the normalized fracture efficiency parameter is larger than 0.65, the error is smaller than 20%. When the normalized fracture efficiency parameter is smaller than 0.65, the error increases significantly. In the study by Kim *et al.*, it was found that an apparent adhesion of 500 J/m$^2$ can be found in the peeling of a 17-$\mu$m-thick copper film while the correct adhesion was believed to be 5 J/m$^2$ after properly accounting for the yielding in the copper film.

Although the examples in Figs 12 and 13 suggest that there may exist certain ranges of normalized fracture efficiency parameter that result in an acceptable error when using $G_{el}$, the range of an acceptable normalized fracture efficiency parameter strongly depends on the test geometry and loading condition. For example, in a 0° peel test for an elastic-perfectly plastic material, there is no acceptable normalized fracture efficiency parameter smaller than 1 because once the specimen yields, it will yield throughout the debonded portion and may result in rupture before debonding. Therefore, when one interprets the experimental results with a normalized fracture efficiency parameter smaller than unity, one needs to properly assess the effect of test geometry and loading condition to determine the error if the analysis for the energy release rate is based on an elastic solution.

## CONCLUSIONS

This paper reports the use of a novel concept, the fracture efficiency, to evaluate adhesive fracture tests by deciding whether a particular test would be more or less likely to cause general yielding or rupturing in the adherend/coating before the fracture condition is satisfied. The methodology presented in this paper not only can be used as the first step to choose among various testing configurations, but can also be used to evaluate whether the measured debond energy is valid within the theory of linear elastic fracture mechanics.

The fracture efficiency and mode mixity for a general coating delamination configuration have been investigated. The results are believed to cover most fracture tests for coating adhesion. A theoretical limit of the fracture efficiency was found, suggesting that yielding or rupturing in a coating may not be prevented, regardless of the test method, without substantially increasing the coating thickness or adding a backing on the coating. Experimental or analytical techniques considering the inelastic energy dissipation may be needed for coating adhesion measurement. The results also suggest that it was unlikely to devise a new test with a significantly higher fracture efficiency than the existing tests. A study of the phase angle not only showed the fracture mode mixities of general coating delamination configurations, but also the conditions which might result in the contact of the crack surfaces near the crack tip region. The result provides a convenient method to decide whether a particular test would be more or less likely to debond the coating interfacially. In this paper, the dependency of the fracture efficiency on the mode mixity is demonstrated through a comparison of four laminated beam specimens with different fracture modes. The comparison suggested that the double cantilever beam test is the best geometry because of the highest fracture efficiency of the four. Based on the study of the general coating delamination configuration, guidelines were given to aid in the selection and design of appropriate test geometries for coating adhesion measurement from the viewpoint of fracture efficiency.

Finally, the error associated with the use of an elastic analysis when yielding occurs in the adherends was also investigated for the 90° peel and double cantilever beam specimens. While the errors of using elastic solutions increased as the normalized fracture efficiency parameter became smaller than unity for both specimens, the elastic solution for the 90° peel test overestimated the debond energy and that for the double cantilever beam test underestimated the debond energy. Although the error study of the 90° peel and double cantilever beam specimens showed that the elastic analysis could still be applicable in certain normalized fracture efficiency parameter ranges even though the adherend is yielded, the range depended on the test geometry. Once adherend yielding occurs, proper error evaluation should be done based on a nonlinear analysis for that particular specimen design.

*Acknowledgements*—The authors would like to acknowledge the financial support of the National Science Foundation's Science and Technology Center on High Performance Polymeric Adhesives and Composites at Virginia Tech (Contract DMR 9120004), the Center for Adhesive and Sealant Science at Virginia Tech, and the ALCOA Foundation.

## REFERENCES

Allen, M. G. and Senturia, S. D. (1988). Analysis of critical debonding pressures of stressed thin film in the blister test. *J. Adhesion* **25,** 303–315.

Allen, M. G. and Senturia, S. D. (1989). Application of the island blister test for thin film adhesion measurement. *J. Adhesion* **29,** 219–231.

Anderson G. P., Bennett, S. J. and DeVries, K. L. (1977). *Analysis and Testing of Adhesive Bonds*, Academic Press, New York.

Brinson, H. F. (1990). *Adhesives and Sealants, Engineered Materials Handbook*, Vol. 3, H. F. Brinson, Technical Chairman, ASM International.

Broek, D. (1982). *Elementary Engineering Fracture Mechanics*, Martinus Nijhoff Publishers, The Hague.

Chang, M. D., DeVries, K. L. and Williams, M. L. (1972). The effects of plasticity in adhesive fracture, *J. Adhesion* **4,** 221–231.

Chang, T., Sproat, E. A., Lai, Y. H., Shephard, N. E. and Dillard, D. A. (1996). Testing methods for accelerated humidity conditioning and estimation of adhesive bond durability. *J. Adhesion* (in press).

Farris, R. J. and Bauer, C. L. (1988). A self-delamination method of measuring the surface energy of adhesion of coatings. *J. Adhesion* **26,** 293–300.

Gent, A. N. and Hamed, G. R. (1975). Peel mechanics. *J. Adhesion* **7,** 91–95.

Gent, A. N. and Kaang, S. Y. (1986). Pull-off forces for adhesive tapes. *J. Appl. Polym. Sci.* **32,** 4689–4700.

Hutchinson, J. W. and Suo, Z. (1992). Mixed mode cracking in layered materials. In *Advances in Applied Mechanics* (eds J. W. Hutchinson and T. Y. Wu), pp. 63–191, Academic Press, New York.

Kim, K. S. and Kim, J. (1988). Elasto-plastic analysis of the peel test for thin film adhesion. *Trans, ASME, J. Engng Mater. Tech.* **110,** 266–273.

Kim, J., Kim, K. S. and Kim, Y. H. (1989). Mechanical effects in peel adhesion test. *J. Adhesion Sci. Tech.* **3,** 175–187.

Kinloch, A. J., Lau, C. C. and Williams, J. G. (1994). The peeling of flexible laminates. *Int. J. Fracture* **66,** 45–70.

Lai, Y. H. and Dillard, D. A. (1994). A study of fracture efficiency parameter of blister tests for films and coatings. *J. Adhesion Sci. Techn.* **8,** 663–478.

Lai, Y. H. and Dillard, D. A. (1996). The cracked lap shear specimen revisited—a closed form solution. *Int. J. Solids Structures* **33,** 1725–1743.

Ritter, J. E. and Rosenfeld, J. G. (1990). Use of the indentation technique for studying delamination of polymeric coatings. *J. Adhesion Sci. Tech.* **4,** 551–571.

Suo, Z. and Hutchinson, J. W. (1989). Sandwich test specimens for measuring interface crack toughness. *Mat. Sci. Engng* **A107,** 135–143.

Thouless, M. D. and Jensen, H. M. (1992). Elastic fracture mechanics of the peel-test geometry. *J. Adhesion* **38,** 185–197.

Thouless, M. D., Hutchinson, J. W. and Liniger, E. G. (1992). Plane-strain, buckling-driven delamination of thin films: model experiments and mode-II fracture. *Acta Metall. Mat.* **40,** 2639–2649.